Front. Phys. 11(6), 114702 (2016)
DOI 10.1007/s11467-016-0587-0

RESEARCH ARTICLE

Shape effect of nanochannels on water mobility

Guo-Xi Nie[1,*], **Yu Wang**[2,†], **Ji-Ping Huang**[1,‡]

[1] *Department of Physics, State Key Laboratory of Surface Physics, and Collaborative Innovation Center of Advanced Microstructures, Fudan University, Shanghai 200433, China*
[2] *Department of Physics, Zhejiang Agriculture and Forestry University, Hangzhou 311300, China*
*E-mail: *gnie13@fudan.edu.cn, †yuwang_zafu@126.com, ‡jphuang@fudan.edu.cn*
Received February 20, 2016; Accepted March 14, 2016

Confinement can induce unusual behaviors of water. Inspired by the fabrication of carbon nanotubes with noncircular cross sections, we performed molecular dynamics simulations to investigate the mobilities of water confined in carbon nanochannels with circular, square, and equilateral triangular cross sections over a variety of dimensions. We find that water exhibits disparate mobilities across different types of channels below 0.796 nm^2. Notably, compared with the other two channels, water in equilateral triangular channels displays the greatest mobilities. Moreover, at 0.425 nm^2, different ordered structures are found in the three channels, and water inside the square channel exhibits an extremely low mobility. It is also found that above 0.796 nm^2, the mobilities along the tube axis of water converge to that of the bulk. These phenomena are understood by analyzing the structure, dynamics, and hydrogen bonding of water. Our work explores the mobilities of water across noncircular carbon nanochannels, which may expand the prospect of noncircular nanochannels in scientific studies and practical applications, such as desalination and drug delivery.

Keywords molecular dynamics simulations, mobility, noncircular, nanochannel, water

PACS numbers 47.61.-k, 61.20.Ja

Frontiers of Physics

1 Introduction

The study on water mobility across nanochannels has a fundamental meaning in biological activities [1–4] and industrial applications [5–7]. Nanotubular materials have unique water transport properties that have the potential to advance desalination [8–10], ion sieving [11, 12] and drug delivery [13, 14]. Moreover, the behaviors of water inside a carbon nanotube are similar to those in biological water channels [15–21]. Because of this novel similarity, carbon nanotubes have usually acted as model systems to explore behaviors of biological water channels [7, 19–25].

It has been widely believed that external conditions and dimensions of nanochannels can greatly affect water mobilities. Many external conditions (e.g., adding mechanic forces or electric fields [16, 20–22, 26–29]) have received much attention for studying water mobility through nanochannels. Wang *et al.* [16] found that the linearly gradient electric field can pump water molecules passing through a single-walled carbon nanotube fast and unidirectionally. Li *et al.* [21] achieved electro-gating to adjust water transport using a single external charge. Meanwhile, confined water often displays anomalous behaviors compared to the bulk. Based on molecular dynamics simulations of water in carbon nanotubes at high pressures, Koga *et al.* [30] predicted new ice phases, which are not seen in bulk ice, and implied the immobility of water inside nanochannels. These predicted ice structures of water were then observed. Pentagonal to octagonal ring formations of water below 190 K were observed using X-ray diffraction [31]. Mashl *et al.* [32] even found a six-chain ice-like ordered phase of water with a low mobility at room temperature. These studies are all based on carbon nanotubes with circular cross sections.

In practice, nanochannels with noncircular cross sections are indispensable as well [33–36]. For example, the metal-organic materials with square pores were widely used in gas separation [33, 34, 36] and zeolite was applied for dehydration of natural gas [35]. Importantly, the cross sections of biological water nanochannels are generally noncircular as a result of natural selection [37]. Zhu *et al.* studied water transport across two-dimensional nanopores under external pressure and found the transition of water transport from continuum pattern to dis-

crete pattern with pore size decreasing [38]. Also, they utilized a γ-graphyne-4 membrane with triangular pores to achieve 100% salt rejection and a much higher water permeability than that of prevailing commercial membranes and the state-of-the-art nanoporous graphene [39]. Owing to the development of fabrication technologies, carbon nanotubes with noncircular cross sections have been synthesized in recent years. Yanagishita *et al.* [40] described the chemical vapor deposition synthesis of carbon nanotubes with triangular cross sections, which were fabricated using anodic porous alumina with triangular openings as the template. The carbon nanotube with a diamond-shaped cross section was also synthesized in the pores of mica membranes by Xu *et al.* [41] utilizing the chemical vapor deposition method. In addition, other techniques for shaping cross sections of carbon nanotubes have been developed (e.g., with pressure [42, 43], using an electron beam [44], or via selective hydrogenation [45]). Compared to nanotubes with circular cross sections, the noncircular nanochannels are expected to alter the electronic properties of carbon nanotubes [40–42]. However, how cross-sectional shapes affect water mobilities has rarely been investigated. The fabrication of noncircular cross-sectional carbon nanotubes inspired us to investigate the effect of cross-sectional shape on water mobilities across nanochannels based on carbon nanotubes. In this work, we chose noncircular carbon nanochannels with square and equilateral triangular cross sections, and we compared their water mobilities to that of the single-walled carbon nanotubes with circular cross sections, over a variety of dimensions.

2 Method

Our work is based on molecular dynamics simulations, which have been widely used for studying water dynamics in single-walled carbon nanotubes [16] and proteins [2]. The simulation frameworks are shown in Fig. 1(a). Uncapped carbon nanochannels with circular, square, and equilateral triangular cross sections are fixed between two graphene sheets with a separation width of 2.442 nm. The two ends of the nanochannel are located at the same positions along the Z axis as the two graphene sheets [46]. Some carbon atoms are removed from the graphene sheet to form a hole, where the distances between the edge of the hole and the wall of the nanochannel are kept at ≈0.3 nm, thus enabling the graphene sheets to prevent water from appearing outside the nanochannel between the two sheets. Without an external pressure difference, water molecules enter or exit the nanochannel through either of its openings under the effect of thermal fluctuation [46]. For circular nanochannels, armchair single-walled carbon nanotubes [8, 9, 47] of $(6,6),(7,7),\ldots,(12,12)$ are utilized; these range from 0.172 to 1.279 nm^2 in cross-sectional area as measured with the inner van der Waals surfaces. The square and equilateral triangular nanochannels are constructed of graphite sheets [see Fig. 1(b)]. Their cross-sectional areas are set in the same way and their dimensions are equal to those of the circular nanochannels. The corresponding values are listed in Table 1. For each system, the density of water is kept at 1 g/cm^3.

To perform our simulations, we chose a canonical ensemble at room temperature (300 K) and used the molecular dynamics package Gromacs 4.0.7 [48]. Here, the extended simple point charge (SPC/E) water model [49] was chosen to describe water molecules, and water-wall interactions are treated by using the Lennard–Jones (LJ) potential, $V_{LJ} = 4\varepsilon[(\frac{\sigma}{r})^{12} - (\frac{\sigma}{r})^{6}]$, where the values of ε and σ come from Ref. [19]. The cutoff distance for LJ interactions is 1.4 nm. Electrostatic interactions are computed by using the particle-mesh Ewald method [50] (with a real-space cutoff of 0.9 nm and reciprocal space

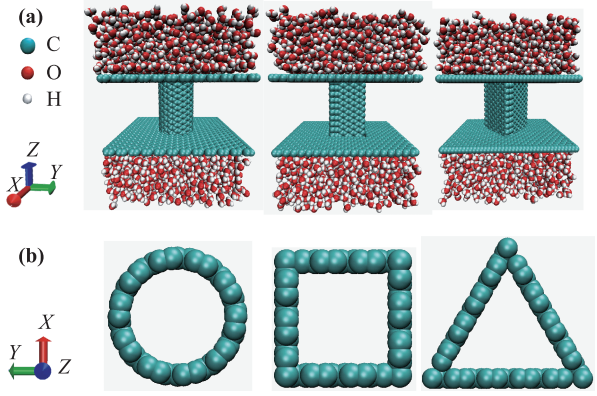

Fig. 1 **(a)** Perspective view of the simulation system with circular, square, and equilateral triangular carbon channels embedded between two parallel graphite sheets. The three different atoms, H (hydrogen), O (oxygen), and C (carbon), are indicated. More details can be found in the main text. **(b)** Cross sections of circular, square, and equilateral triangular channels corresponding to (a); the square and equilateral triangular channels are constructed with four and three graphite sheets, respectively.

Table 1 Channel geometries.

Circular channel geometry	van der Waals cross-sectional area (nm^2)
(6,6)	0.172
(7,7)	0.285
(8,8)	0.425
(9,9)	0.597
(10,10)	0.796
(11,11)	1.022
(12,12)	1.279

gridding of 0.12 nm and fourth-order interpolation). We also adopted the thermostat of Nosé and Hoover [51, 52] with a time constant of 0.5 ps. Periodic boundaries were set in a simulation box with dimensions L_X, L_Y, and L_Z, where $L_X = 4.762$ nm, $L_Y = 5.006$ nm, and $L_Z = 6.442$ nm. In our simulations, a time step of 2 fs was used. The simulation of each system runs for 80 ns, and the last 70 ns of data are collected for analysis.

3 Results and discussion

We graph the diffusion coefficients of water along the tube axis (D_Z) with respect to cross-sectional areas (S) to measure water mobilities inside the three kinds of nanochannels, respectively, as shown in Fig. 2. When $S < 0.796$ nm^2, D_Z values deviate significantly from the value of bulk water and are disparate among different types of nanochannels. Generally, water inside the triangular channel has the highest mobility. In particular, there are sharp reductions of water mobilities for all channels at 0.425 nm^2, while the square channel has a much lower mobility than the other two. However, at 0.597 nm^2, the circular channel exhibits the lowest mobility. As $S \geq 0.796$ nm^2, the values of D_Z converge to that of the bulk, which indicates that water inside the nanochannels starts to behave like bulk water.

To get an overview of what occurs, the cross-sectional snapshots of water inhabiting the nanochannels are displayed in Fig. 3. Here, those cases whose cross sections are larger than 0.796 nm^2 are not shown, since their behaviors are similar to those of 0.796 nm^2. In circular channels, water displays the same structures as found in

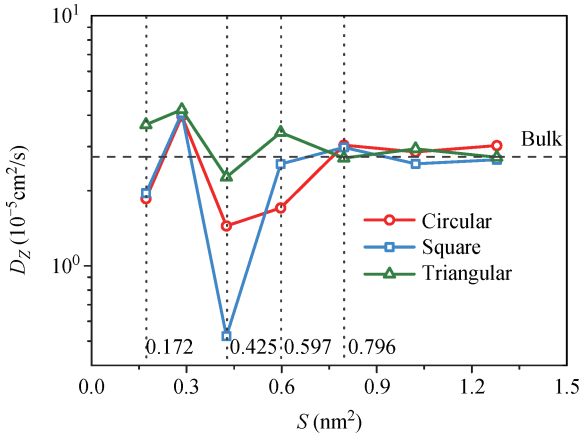

Fig. 2 Profile of the diffusion coefficient of water molecules along the Z axis (channel axis), D_Z, for the circular, square, and triangular channels over a variety of dimensions. The dashed line presents the diffusion coefficient along the Z axis of bulk water; the specific dimensions, 0.172, 0.425, 0.597, and 0.796, are also indicated.

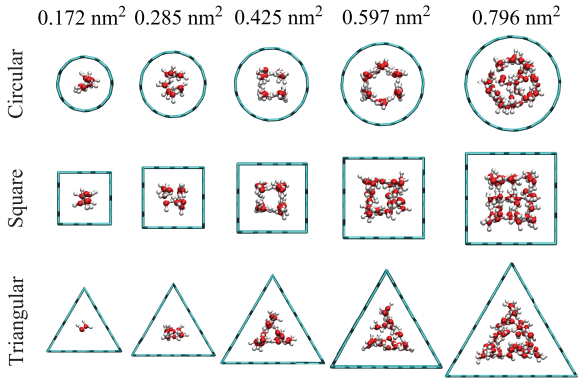

Fig. 3 Cross-sectional snapshots of water structures in the circular, square, and triangular channels with $S = 0.172$ to 0.796 nm^2.

previous works (e.g., the single-chain structure in (6,6) carbon nanotubes [16] (at 0.172 nm^2), the four-chain or square ice-like structure in (8,8) carbon nanotubes [53] (at 0.425 nm^2), and the six-chain structure or hexagonal ice-like structure [32] in (9,9) carbon nanotubes (at 0.597 nm^2)). The ice-like structures are believed to have lower mobilities [32, 53]. Interestingly, in our work, a four-chain structure is also found in the square channel at 0.425 nm^2, and a three-chain structure forms inside the triangular channel. However, at 0.597 nm^2, no such ordered structures are found in noncircular channels. Above 0.796 nm^2, water in all cases behaves like the bulk. At 0.172 nm^2, in contrast from the stable single-chain structure in circular and square channels, which suggests continuous transport of water, water molecules discontinuously appear inside the triangular channel. Figure 4(a) presents the number of water molecules, $N(t)$, inside the nanochannels when $S = 0.172$ nm^2 as a function of time. Compared to the filled states in circular and square channels, water in a triangular channel exhibits filled and empty states; this is similar to the phenomenon observed in Ref. [19] when the attraction between carbon and water molecules is reduced. That is, under the strong confinement of a triangular channel, water chains are unstable and easily break, making it easy to empty the channel.

Figure 4(b) shows a plot of the probability distribution of the number of water molecules (N) inside the channels over a variety of dimensions. In general, within the same dimension, there is little difference of N among the three kinds of channels, but the circular one still accommodates the most water molecules, and the triangular channels contain the least, which is attributed to the strong confinement induced by corners in the noncircular channels. Note that, at 0.425 nm^2, N in the square channel exhibits a more concentrated distribution, suggesting a more stable water structure.

A better understanding of the differences in water mo-

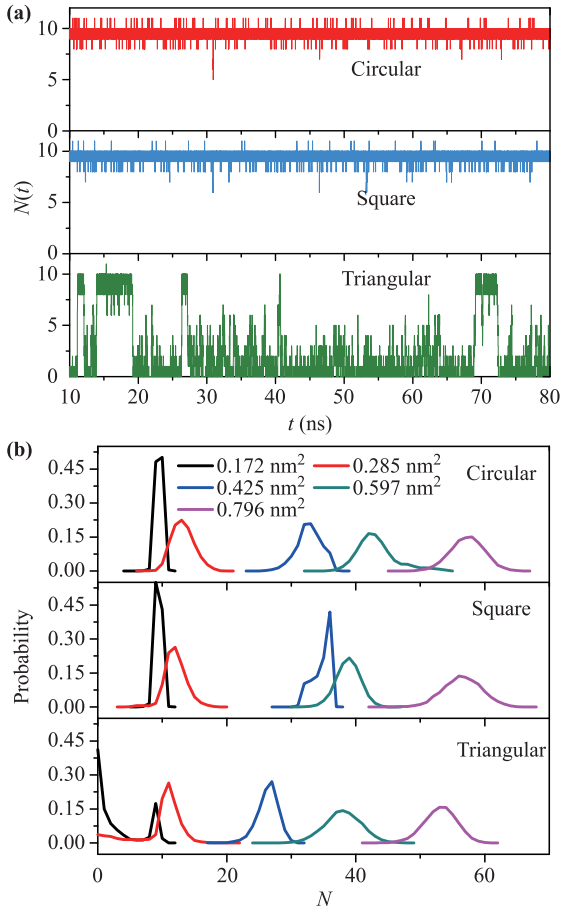

Fig. 4 **(a)** Number of water molecules, $N(t)$, inside the circular, square, and triangular nanochannels of 0.172 nm^2 as a function of time. **(b)** Probability distribution of water molecules in the circular, square, and triangular channels with $S = 0.172$ to 0.796 nm^2.

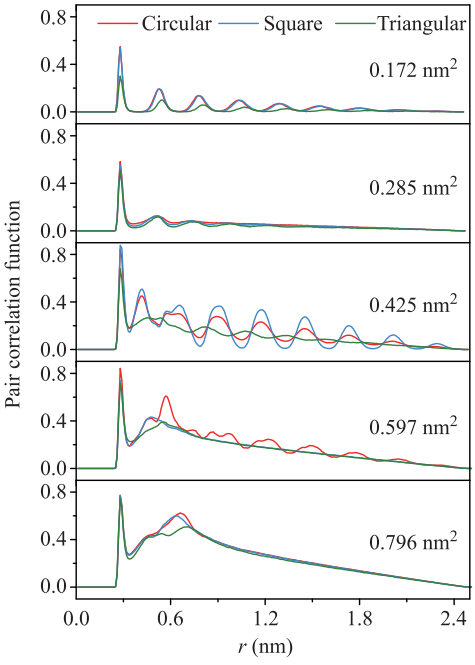

Fig. 5 Profile of the pair correlation functions of water molecules in the circular, square, and triangular channels with $S = 0.172$ to 0.796 nm^2.

bilities among the three kinds of channels requires insight into water structures. To quantify how water molecules arrange, we contrast the pair correlation functions of water inside the three channels (see Fig. 5). Below 0.597 nm^2, water structures exhibit solid-like characteristics, owing to the wave-like distribution. At 0.172 nm^2, the less ordered structure of water inside the triangular channel corresponds to its higher mobility. At 0.285 nm^2, water structures in the three channels are similar to each other and the mobilities are close to each other. As $S = 0.425$ nm^2, water displays stronger solid-like characteristics, with the structure in the square channel being most solid-like, thus water in it diffuses least. However, when $S = 0.597$ nm^2, only the water in the circular channel remains solid-like and retains a low mobility. As the dimension increases futher, all water structures exhibit liquid characteristics. Such results correspond well with the phenomena from Figs. 2 and 3.

We also average the number densities of oxygen and hydrogen atoms across the cross sections over 70 ns, respectively, and the two-dimensional density maps are graphed in Fig. 6. Obviously, the cross-sectional shapes have substantial effects on the water structures. Owing to the confinement of the noncircular walls, water molecules exhibit an anisotropic distribution, and they tend to concentrate at the corners. In contrast, water is distributed uniformly along the walls of circular channels. As dimensions become larger, water structures come close to that of the bulk. It should be noted that, although water chains (see Fig. 3) form in the circular (at 0.425 and 0.597 nm^2), square (at 0.425 nm^2), and triangular (at 0.425 nm^2) channels, they behave differently. We find that the ordered structure in circular channels can rotate along the walls, which is evidenced by water's uniform distribution along the walls. However, owing to the strong confinement from corners, such an ordered structure cannot rotate along the walls of square or triangular channels. Water molecules are restrained by the confinement and quiver at the corners of noncircular channels. In the triangular channel, water molecules oscillate in a larger area compared to that in the square one. The stability of the water structure in the square channel indicates the prominent solid-like feature, while the rotation in the circular channel and stronger oscillation in the triangular channel are manifestations of the less solid-like characteristics of water structures.

To study the hydrogen bonding capability of water inhabiting the nanochannels, we calculated the average

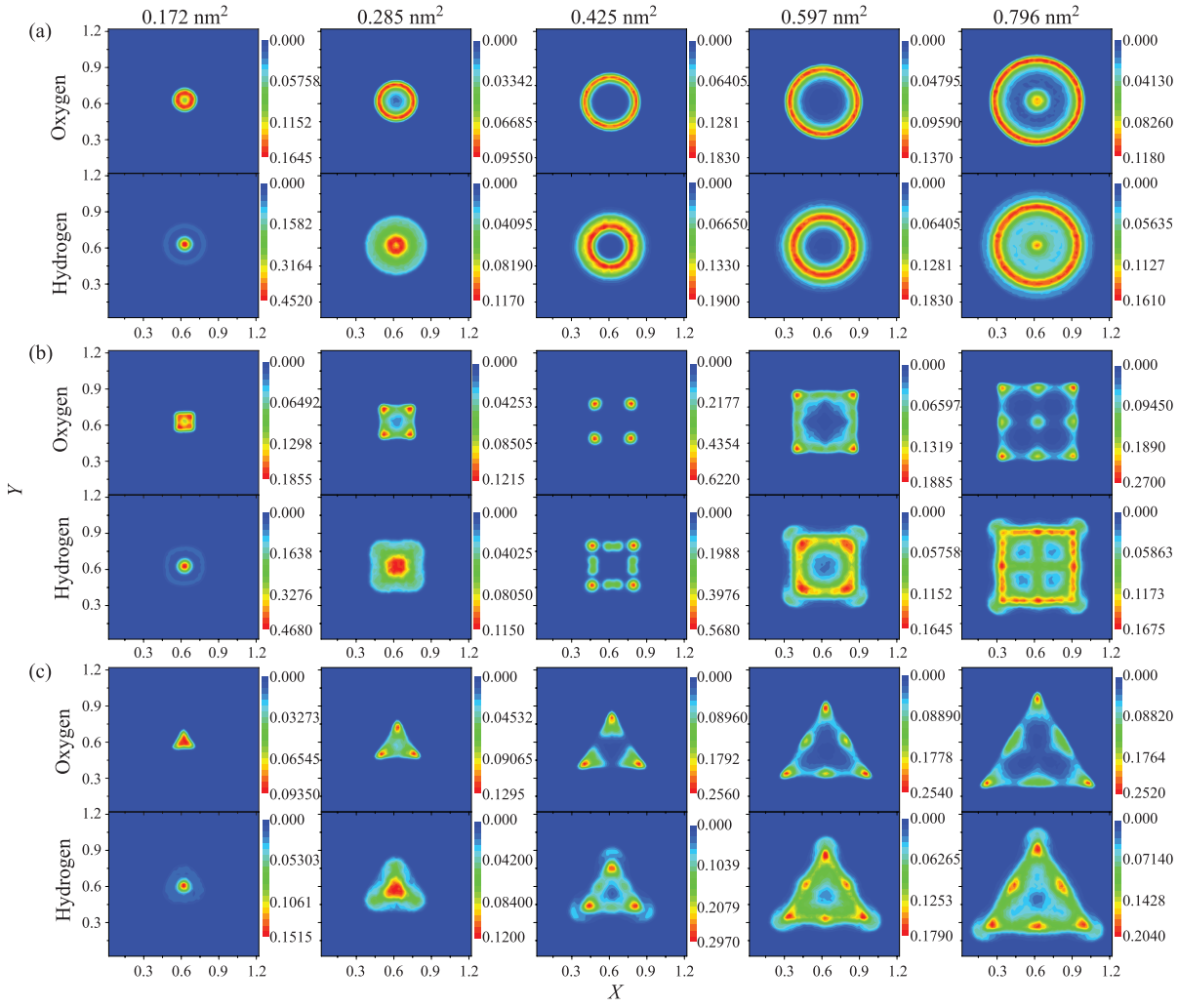

Fig. 6 Cross-sectional two-dimensional density maps of oxygen and hydrogen atoms in the circular, square, and triangular channels with $S = 0.172$ to 0.796 nm^2.

number of hydrogen bonds (H bonds) around each water molecule. An H bond exists if the donor–acceptor distance is within 0.35 nm, which is the first minimum of the radial distribution function for the oxygen atoms in bulk water, and the orientation of the O–H donor bond is within 30° of the acceptor oxygen. The results are shown in Fig. 7(a). Generally, for all three types of channels, as the dimensions increase, there are more H bonds around a water molecule, and the numbers get close to that of the bulk. At 0.425 nm^2, there are remarkably more H bonds around each water molecule in the square channel than in the other two channels, which corresponds to its most pronounced solid-like structure, and fewer H bonds than in the circular channel at 0.597 nm^2 with the solid-like structure disappearing. Within the same dimension as $S \leq 0.597$ nm^2, there are obviously fewer H bonds for each water molecule in the triangular channels, leading to the weakest restriction between water molecules. It should be noticed that the number of water molecules in the first hydration shell, which is within 0.35 nm to a candidate molecule, is the least in the triangular channel (see Fig. 5). Fewer water molecules around a candidate molecule within 0.35 nm lead to weaker hydrogen bonding.

For clarifying the relationship between water mobility and the H bond networks, we studied the orientation of H bonds inside the nanochannels. We define $P(\theta)$ as the probability function for the angle between an H bond and the channel axis, which is denoted by θ ($0° \leq \theta \leq 90°$). Another quantity, $N_{HB}(\theta)$, is defined as $N_{HB}(\theta) = P(\theta)\times$ (average number of H bonds per water molecule). Thus, $N_{HB}(\theta)$ shows the average number of H bonds per water molecule along different directions. Figure 7(b) displays $N_{HB}(\theta)$ as a function of θ for the nanochannels over a variety of cross-sectional areas. When $S = 0.172$ nm^2, water inside the circu-

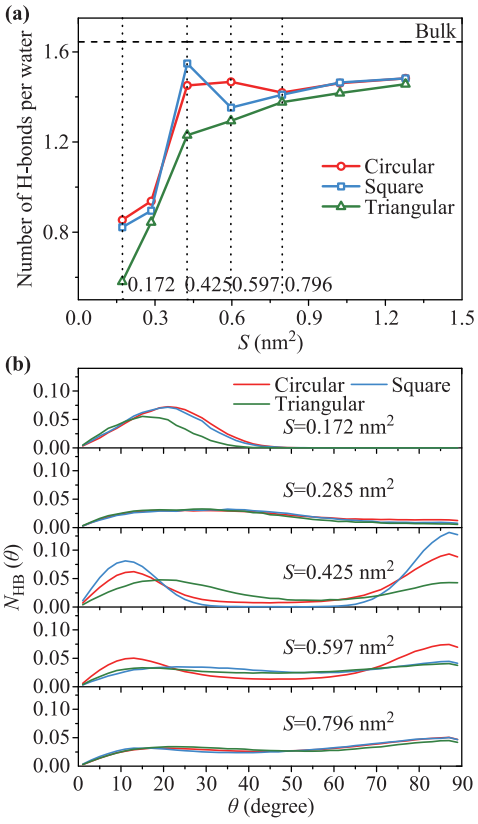

Fig. 7 **(a)** Profile of the number of H bonds per water molecule for the circular, square, and triangular channels over a variety of dimensions. The dashed line presents the value of bulk water; specific dimensions, 0.172, 0.425, 0.597, and 0.796, are indicated. **(b)** Number distribution of H bonds per water molecule inside nanochannels with respect to the angle between an H bond and the channel axis, θ, where $S = 0.172$–0.796 nm^2.

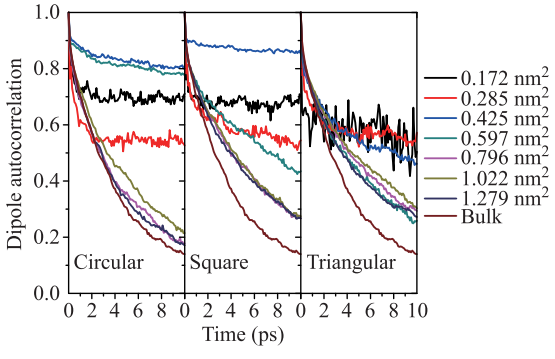

Fig. 8 Water dipole autocorrelation function (ACF) in the circular, square, and triangular channels with a variety of dimensions.

lar nanochannel performs single-file diffusion, and the H bonds align nearly along the channel axis, which can develop the mobility of water [19]. θ values in circular and square channels lie between 0° and 47°. However, owing to a stronger confinement, the H bonds in the triangular channel are more parallel with the channel axis, with θ ranging from 0° to 39°. The larger amount and wider orientation range of H bonds in circular and square channels strengthen the restriction between water molecules and make water more solid-like, reducing water mobility. In contrast, the more parallel tendency of H bonds along the channel axis and the weaker restriction between water molecules in the triangular channel develop water mobility. When the pore size increases, H bonds perpendicular to the channel axis form. At 0.285 nm^2, the similar distributions of H bonds correspond to their close structure and mobilities. When $S = 0.425$ nm^2, there are two peaks for the three channels, respectively, which indicates the ordered structures of water. For the square channel, two peaks are located at 11° and 87°, and these are higher than those in the other two channels. Moreover, between 35° and 57°, there are almost no H bonds. These features manifest the most prominent solid-like characteristic. The water structure is very stable, suggesting the lowest mobility. For the circular channel, two peaks are located at 13° and 87°, and these are lower than the peaks in the square channel. For the triangular channel, the peaks are much flatter, being located at 19° and 87°. Water is the least solid-like, and the restriction between water molecules is much weaker, suggesting a higher mobility. When $S = 0.597$ nm^2, only the circular channel displays an ordered H bond network, which corresponds to a lower water mobility. As the pore size increases more, there are no obvious preferences of H bond orientations, and water displays a liquid-like feature. In general, the prominent preference of H bond orientation orders the water structure, and a larger number of highly ordered H bonds enhances the restriction between water molecules, which reduces water mobilities.

The reorientability of water inside the channels was then examined, using an autocorrelation function (ACF) for water dipoles. The ACF is given by $C(t) = \langle p_i(0) \cdot p_i(t) \rangle / \langle p^2 \rangle$ [32], where p is the water dipole moment, and the angle brackets denote averages over time t and molecules. The result is graphed in Fig. 8, which provides us with the following qualitative understanding. As dimension increases, the ACFs gradually get close to that of the bulk. For the circular (at 0.425 and 0.597 nm^2) and square (at 0.425 nm^2) channels, the appearance of plateaus implies a fast formation of H bonds, and these H bonds can be maintained for a much longer time. Compared with those of the triangular channel, they show a remarkably higher degree of water molecules' rotational immobilization, suggesting a much longer relaxation time scale. Moreover, for the square channel at 0.425 nm^2, H bonds form the fastest, and the rotational motions of water molecules occur within the narrowest range of angles, indicating its more stable structure.

4 Conclusion

We conclude that the structures, dynamics, and hydrogen bonding of water are differentiated at small dimensions by the isotropic and anisotropic confinement of nanochannels owing to the different cross-sectional shapes. Water exhibits disparate mobilities across the three kinds of channels when cross sections are below 0.796 nm^2, especially at 0.425 and 0.597 nm^2. Different ordered structures form in the circular (at 0.425 and 0.597 nm^2), square (0.425 nm^2), and triangular (0.425 nm^2) channels. Because of the weaker restriction between water molecules, water in the triangular channel maintains a higher mobility than in the other two types of channel. In addition, as $S \geq 0.796$ nm^2, water in all channels starts to behave like the bulk.

The present study may provide enlightenment into nano-mechanical engineering with noncircular nanochannels. Moreover, this work can inspire new research on water movement across nanochannels in biological membranes; such nanochannels often have noncircular cross sections because they are constructed of soft matter such as proteins.

Acknowledgements We acknowledge financial support by the National Natural Science Foundation of China under Grant Nos. 11222544 and 11304284 (Y.W.), the Fok Ying Tung Education Foundation under Grant No. 131008, the Program for New Century Excellent Talents in University (Grant No. NCET-12-0121), and the CNKBRSF under Grant No. 2011CB922004. The computational resources utilized in this research were provided by the Shanghai Supercomputer Center.

References

Karttunen2010JPCB. K. Kaszuba, T. Rog, K. Bryl, I. Vattulainen, and M. Karttunen, Molecular dynamics simulations reveal fundamental role of water as factor determining affinity of binding of beta-blocker nebivolol to beta(2)-adrenergic receptor, *J. Phys. Chem. B* 114, 8374 (2010)

2. B. L. de Groot and H. Grubmuller, Water permeation across biological membranes: Mechanism and dynamics of aquaporin-1 and GlpF, *Science* 294, 2353 (2001)
3. X. Gong, J. Li, H. Zhang, R. Wan, H. Lu, S. Wang, and H. P. Fang, Enhancement of water permeation across a nanochannel by the structure outside the channel, *Phys. Rev. Lett.* 101, 257801 (2008)
4. X. Y. Li, Y. C. Shi, Y. L. Yang, H. L. Du, R. H. Zhou, and Y. L. Zhao, How does water-nanotube interaction influence water flow through the nanochannel? *J. Chem. Phys.* 136, 175101 (2012)
5. M. F. L. De Volder, S. H. Tawfick, R. H. Baughman, and A. J. Hart, Carbon nanotubes: Present and future commercial applications, *Science* 339, 535 (2013)
6. D. Cohen-Tanugi and J. C. Grossman, Water desalination across nanoporous graphene, *Nano Lett.* 12, 3602 (2012).
7. R. Z. Wan, J. Y. Li, H. J. Lu, and H. P. Fang, Controllable water channel gating of nanometer dimensions, *J. Am. Chem. Soc.* 127, 7166 (2005)
8. Q. W. Chen, L. Y. Meng, Q. K. Li, D. Wang, W. Guo, Z. G. Shuai, and L. Jiang, Water transport and purification in nanochannels controlled by asymmetric wettability, *Small* 7, 2225 (2011)
9. B. Corry, Water and ion transport through functionalised carbon nanotubes: Implications for desalination technology, *Energy Environ. Sci.* 4, 751 (2011)
10. B. Corry, Designing carbon nanotube membranes for efficient water desalination, *J. Phys. Chem. B* 112, 1427 (2008)
11. X. J. Gong, J. C. Li, K. Xu, J. F. Wang, and H. Yang, A controllable molecular sieve forNa^+ andK^+ ions, *J. Am. Chem. Soc.* 132, 1873 (2010)
12. J. Dzubiella and J. P. Hansen, Electric-field-controlled water and ion permeation of a hydrophobic nanopore, *J. Chem. Phys.* 122, 234706 (2005)
13. T. Panczyk, T. P. Warzocha, and P. J. Camp, A magnetically controlled molecular nanocontainer as a drug delivery system: The effects of carbon nanotube and magnetic nanoparticle parameters from Monte Carlo simulations, *J. Phys. Chem. C* 114, 21299 (2010)
14. Y. L. Zhao, Y. L. Song, W. G. Song, W. Liang, X. Y. Jiang, Z. Y. Tang, H. X. Xu, Z. X. Wei, Y. Q. Liu, M. H. Liu, L. Jiang, X. H. Bao, L. J. Wan, and C. L. Bai, Progress of nanoscience in China, *Front. Phys.* 9, 288 (2014)
15. S. Cambre, B. Schoeters, S. Luyckx, E. Goovaerts, and W. Wenseleers, Experimental observation of single-file water filling of thin single-wall carbon nanotubes down to chiral index (5,3), *Phys. Rev. Lett.* 104, 207401 (2010)
16. Y. Wang, Y. J. Zhao, and J. P. Huang, Giant pumping of single-file water molecules in a carbon nanotube, *J. Phys. Chem. B* 115, 13275 (2011)
17. H. Lu, J. Li, X. Gong, R. Wan, L. Zeng, and H. P. Fang, Water permeation and wavelike density distributions inside narrow nanochannels, *Phys. Rev. B* 77, 174115 (2008)
18. J. Y. Su and H. X. Guo, Control of unidirectional transport of single-file water molecules through carbon nanotubes in an electric field, *ACS Nano* 5, 351 (2011)
19. G. Hummer, J. C. Rasaiah, and J. P. Noworyta, Water conduction through the hydrophobic channel of a carbon nanotube, *Nature* 414, 188 (2001)
20. X. W. Meng, Y. Wang, Y. J. Zhao, and J. P. Huang, Gating of a water nanochannel driven by dipolar molecules, *J. Phys. Chem. B* 115, 4768 (2011)
21. J. Y. Li, X. J. Gong, H. J. Lu, D. Li, and R. H. Zhou, Electrostatic gating of a nanometer water channel, *Proc. Natl. Acad. Sci. USA* 104, 3687 (2007)
22. X. J. Gong, J. Y. Li, H. J. Lu, R. Z. Wan, J. C. Li, J. Hu, and H. P. Fang, A charge-driven molecular water pump, *Nature Nanotech.* 2, 709 (2007)
23. Y. B. Chen, Y. H. Liu, Y. Zeng, W. Mao, L. Hu, Z. L. Mao, and H. Q. Xu, Optimal aspect ratio of endocytosed spherocylindrical nanoparticle, *Front. Phys.* 10, 108702 (2015)
24. R. García-Fandiño and M. S. P. Sansom, Designing biomimetic pores based on carbon nanotubes, *Proc. Natl. Acad. Sci. USA* 109, 6939 (2012)
25. G. X. Guo, L. Zhang, and Y. Zhang, Molecular dynamics study of the infiltration of lipidwrapping C60 and polyhydroxylated single-walled nanotubes into lipid bilayers, *Front. Phys.* 10, 108601 (2015)

26. X. Y. Zhou, F. M. Wu, J. L. Kou, X. C. Nie, Y. Liu, and H. J. Lu, Vibrating-charge-driven water pump controlled by the deformation of the carbon nanotube, *J. Phys. Chem. B* 117, 11681 (2013)
27. R. Qiao and N. R. Aluru, Atypical dependence of electroosmotic transport on surface charge in a single-wall carbon nanotube, *Nano Lett.* 3, 1013 (2003)
28. G. X. Nie, Y. Wang, and J. P. Huang, Role of confinement in water solidification under electric fields, *Front. Phys.* 10, 106101 (2015)
29. T. Qiu and J. P. Huang, Unprecedentedly rapid transport of single-file rolling water molecules, *Front. Phys.* 10, 106102 (2015)
30. K. Koga, G. T. Gao, H. Tanaka, and X. C. Zeng, Formation of ordered ice nanotubes inside carbon nanotubes, *Nature* 412, 802 (2001)
31. Y. Maniwa, H. Kataura, M. Abe, A. Udaka, S. Suzuki, Y. Achiba, H. Kira, K. Matsuda, H. Kadowaki, and Y. Okabe, Ordered water inside carbon nanotubes: Formation of pentagonal to octagonal ice-nanotubes, *Chem. Phys. Lett.* 401, 534 (2005)
32. R. J. Mashl, S. Joseph, N. R. Aluru, and E. Jakobsson, Anomalously immobilized water: A new water phase induced by confinement in nanotubes, *Nano Lett.* 3, 589 (2003)
33. S. R. Venna and M. A. Carreon, Metal organic framework membranes for carbon dioxide separation, *Chem. Eng. Sci.* 124, 3 (2015)
34. P. Nugent, Y. Belmabkhout, S. D. Burd, A. J. Cairns, R. Luebke, K. Forrest, T. Pham, S. Q. Ma, B. Space, L. Wojtas, M. Eddaoudi, and M. J. Zaworotko, Porous materials with optimal adsorption thermodynamics and kinetics forCO_2 separation, *Nature* 495, 80 (2013)
35. S. Shirazian and S. N. Ashrafizadeh, Synthesis of substrate-modified LTA zeolite membranes for dehydration of natural gas, *Fuel* 148, 112 (2015)
36. G. Sneddon, A. Greenaway, and H. H. P. Yiu, The potential applications of nanoporous materials for the adsorption, separation, and catalytic conversion of carbon dioxide, *Adv. Energy Mater.* 4, 1301873 (2014)
37. K. Murata, K. Mitsuoka, T. Hirai, T. Walz, P. Agre, J. B. Heymann, A. Engel, and Y. Fujiyoshi, Structural determinants of water permeation through aquaporin-1, *Nature* 407, 599 (2000)
38. C. Q. Zhu, H. Li, and S. Meng, Transport behavior of water molecules through two-dimensional nanopores, *J. Phys. Chem.* 141, 18C528 (2014)
39. C. Q. Zhu, H. Li, X. C. Zeng, E. G. Wang, and S. Meng, Quantized water transport: Ideal desalination through graphyne-4 membrane, *Sci. Rep.* 3, 3163 (2013)
40. T. Yanagishita, M. Sasaki, K. Nishio, and H. Masuda, Carbon nanotubes with a triangular cross-section, fabricated using anodic porous alumina as the template, *Adv. Mater.* 16, 429 (2004)
41. F. Xu, J. E. Wharton, and C. R. Martin, Template synthesis of carbon nanotubes with diamond-shaped cross sections, *Small* 3, 1718 (2007)
42. J. Zang, A. Treibergs, Y. Han, and F. Liu, Geometric constant defining shape transitions of carbon nanotubes under pressure, *Phys. Rev. Lett.* 92, 105501 (2004)
43. W. H. Mu, J. S. Cao, and Z. C. Ou-Yang, Shape transition of unstrained flattest single-walled carbon nanotubes under pressure, *J. Appl. Phys.* 115, 044512 (2014)
44. A. Zobelli, A. Gloter, C. P. Ewels, and C. Colliex, Shaping single walled nanotubes with an electron beam, *Phys. Rev. B* 77, 045410 (2008)
45. G. F. Wu, J. L. Wang, X. C. Zeng, H. Hu, and F. Ding, Controlling cross section of carbon nanotubes via selective hydrogenation, *J. Phys. Chem. C* 114, 11753 (2010)
46. T. Qiu, X. W. Meng, and J. P. Huang, Nonstraight nanochannels transfer water faster than straight nanochannels, *J. Phys. Chem. B* 119, 1496 (2015)
47. L. Hao, J. Y. Su, and H. X. Guo, Water permeation through a charged channel, *J. Phys. Chem. B* 117, 7685 (2013)
48. B. Hess, C. Kutzner, D. Van De Spoel, and E. Lindahl, GROMACS 4: Algorithms for highly efficient, load-balanced, and scalable molecular simulation, *J. Chem. Theory. Comp.* 4, 435 (2008)
49. H. J. C. Berendsen, J. R. Grigera, and T. P. Straatsma, The missing term in effective pair potentials, *J. Phys. Chem.* 91, 6269 (1987)
50. T. A. Darden, D. M. York, and L. G. Pedersen, Particle mesh Ewald: An N-log(N) method for Ewald sums in large systems, *J. Chem. Phys.* 98, 10089 (1993)
51. S. Nosé, A unified formulation of the constant temperature molecular dynamics methods, *J. Chem. Phys.* 81, 511 (1984)
52. W. G. Hoover, Canonical dynamics: Equilibrium phase-space distributions, *Phys. Rev. A* 31, 1695 (1985)
53. Z. J. He, J. Zhou, X. H. Lu, and B. Corry, Ice-like water structure in carbon nanotube (8,8) induces cationic hydration enhancement, *J. Phys. Chem. C* 117, 11412 (2013)